2011 IEEE/RSJ International Conference on
Intelligent Robots and Systems
September 25-30, 2011. San Francisco, CA, USA

Caging Grasps for Micromanipulation & Microassembly

David J. Cappelleri, Michael Fatovic, and Zhenbo Fu

Abstract— **In this paper, we demonstrate a systematic way to determine configurations for up to four coordinated micro-manipulators to form caging grasps for transporting micro-scale planar, polygonal parts. We exploit the geometry of the part, noting the presence and location of convex corners and non-convex corners, and form opposing force equivalents with the micromanipulator probe tips around the micro-scale parts that define a caging polygon. We perform an error bound analysis for caging grasps derived in this manner and provide theoretical values of this bound for four micro-parts of interest. We demonstrate experimental results of the caging micromanipulation transport primitive using these feature-defined grasps and compare them with the expected error bounds. Finally, we combine this caging transport primitive along with rotational and one-sided-pushing motion primitives, to carry out a representative microassembly task.**

I. INTRODUCTION

In recent years as the push to create smaller and cheaper products with increased throughput, research on gripping and manipulation techniques for microassembly applications is becoming more important and prevalent in the research community [1]. There is a large body of work pertaining to pick-and-place microassembly tasks using micro-gripping techniques and strategies [2], [3], [4], [5], [6], [7], [8]. Sticking effects due to Van der Walls forces and static electricity make the manipulator motions and part release at the micro-scale more complicated than at the macro-scale [9], [10]. Manipulators at the micro-scale are also limited in their degrees-of-freedom when compared to their macro-scale counterparts [11]. In this work, rather than focusing on pick-and-place micro-assembly tasks with microgrippers, we are interested in using micro-scale pushing operations. This approach is more suitable for open loop or quasi-open loop (feedback only a discrete intervals) manipulations which can be used to solve generic microassembly problems, like the one shown in Fig. 1.

For nonprehensile manipulation (manipulation without grasping), extensive studies have been explored to derive the fundamental mechanics of sliding objects and pushing operations [12], [13], [14], [15]. There is also extensive work addressing the analysis and simulation of mechanical systems with frictional contacts [16], [17]. The problem of finding motion primitives that rely on pushing and are robust to errors has received significant attention [18], [19], [20]. All of this work is focused at the macro-scale. At the micro-scale, various strategies and techniques for manipulation have been investigated and are documented in [21]. However, prior work addressing micromanipulation with real-time sensor feedback is limited. This is mainly because obtaining accurate sensor data is extremely difficult at this scale.

D. Cappelleri, M. Fatovic, and Z. Fu and are with the Multi-Scale Robotics and Automation Lab, Department of Mechanical Engineering, Stevens Institute of Technology, 1 Castle Point on Hudson, Hoboken, NJ USA 07030 [dcappell, zfu, mfatovic] @stevens.edu

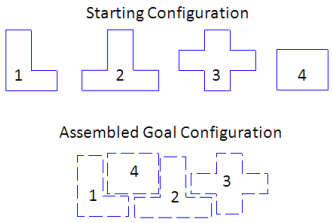

Fig. 1. Representative microassembly problem: manipulate micro-scale parts from their initial configuration to the assembled goal configuration.

Sensors cannot easily be affixed to tiny precision instruments without compromising their functionality [10]. The use of high resolution optical systems with controllable parameters for microassembly tasks are examined in [22]. Even with this sensor data, calibration and vision-based control at this scale is difficult. Without accurate sensor data, it is hard to develop models, and therefore controllers, for micromanipulation.

Previous work on cooperative manipulation has utilized the concepts of form and force closure to manipulate large macro-scale objects [23], [24], [25]. It is possible to use conditional force closure to transport an object by pushing it from an initial position to a goal position [26], [20]. Conditional force closure makes use of both the manipulation forces generated by contacts from the robots as well as the external forces acting on the object, such as friction and gravity. Object closure or caging is variation of this. It only requires that the objected be caged by the robots and confined to a compact set in the configuration space [27], [28]. Multirobot manipulation of non-circular objects and cooperative manipulation in environments with obstacles has been demonstrated in [28], [29] with macro-scale mobile robots. We have recently used similar principles and applied them to micromanipulation and assembly tasks, creating a new micro-scale caging transport primitive [30]. We coupled this primitive with our prior work [31], [32], [33] and [34] to construct rotational and 1D translation motion primitives to use with this caging transport primitive to carry out a sample microassembly task. In that study, we learned that a simple caging circle is not adequate to ensure reliable control of the state of the micro-part during transport and that a tight cage, based on the part geometrical features is needed instead. In this paper, we explore how we can exploit the geometry of different types of planar micro-scale parts in order to systematically plan reliable caging grasps for the micro-scale caging transport primitive. We estimate the error bounds on the state of the part during transport. Finally, we use these caging grasps in the caging transport primitive, along with rotational and one-sided-pushing motion primitives, to carry out the microassembly task in Fig. 1.

II. PROBLEM FORMULATION

The problem formulation from our previous work in [30] remains the same here. We consider a group of N micro-

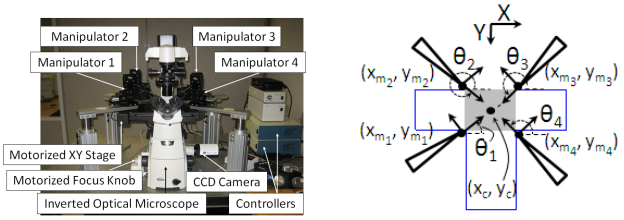

(a) Microrobotics test-bed (b) Local micromanipulator coordinates on a caging polygon

Fig. 2. Test-bed and micromanipulator positioning for caging transport.

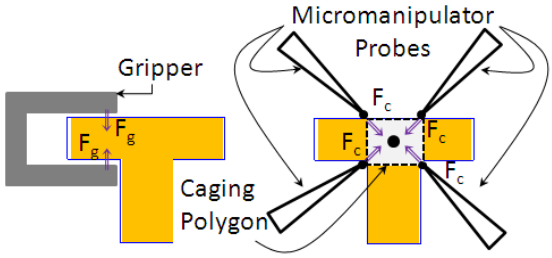

Fig. 3. Parallel jaw grippers (left) and Feature-defined (FD) cage (right) grasping parts. Both utilize symmetric force equivalents to control the state of the part.

manipulators ($N \leq 4$) with single point probes (robots) operating in the XY plane with kinematics given by: $\dot{q}_{m_i} = u_{m_i}$ where $q_{m_i} = (x_{m_i}, y_{m_i})^T$ and u_{m_i} denote the i^{th} tip position of the manipulator's probe and corresponding control input. We assume each manipulator is localized in a global coordinate frame. Our objective is to design a set of control inputs to enable a team of N micromanipulators to surround and transport an object to a desired location and orientation while avoiding obstacles in the environment in order to solve the representative microassembly problem depicted in Fig.1.

III. CAGING GRASPS FOR ROBUST TRANSPORT

A. Caging Transport

When using caging micromanipulation for transporting a micro-part of interest, we assume that if the cage is maintained, the part's centroid, (x_p, y_p), will always lie within a caging polygon. Guarantees of part rotation are not made but they can be bounded utilizing caging parameters driven by the part geometries, which will be described shortly. The microrobotics test-bed used here (Fig. 2(a)) allows for use of up to *N* = 4 manipulators for micro-scale caging transport operations, as seen in Fig. 2(b).

To translate the center position of the cage, (x_c, y_c), we must map the control inputs, $U_{cage} = [u_{x_c} u_{y_c} 0]^T$, to the local frames of the micromanipulators being utilized. Each manipulator control input, u_{m_i}, must be prescribed in the local coordinate frame orthogonal to the manipulator's orientation (θ_i, i = 1,..,4, as defined in Fig. 2(b)) and are given by: $u_{m_i} = T_i U_{cage} = [u_{x_{m_i}} u_{y_{m_i}} u_{z_{m_i}}]^T$, where T_i corresponds to the transformation matrix for each manipulator: $T_1 = R_x(180°)R_z(\theta_1)$, $T_2 = R_x(180°)R_z(\theta_2)$, $T_3 = R_z(\theta_3)$, and $T_4 = R_z(\theta_4)$. In these expressions, $R_x(\beta)$ and $R_z(\beta)$ represent 3D-rotation matrices about the x and z axes, respectively, by the prescribed angle β [35].

B. Determining Grasps for a Feature-Defined (FD) Cage

In this paper, we are interested in systematically determining configurations for the N micromanipulators in order to form a caging grasps for transporting micro-scale planar, polygonal parts. Previous work [28] utilizing macro-scale robots for caging manipulations have simply defined a caging circle around the part to accomplish this task in the following way: Assume a convex workspace $\mathcal{W}$ with a boundary denoted by $\partial\mathcal{W}$. Given a part whose centroid is denoted as (x_p, y_p), we assume there exists a smooth shape, $\mathcal{S}$, whose boundary, $\partial\mathcal{S}$, is a smooth, regular, closed curve with the form $s(x, y) = 0$ such that the part is contained within $\partial\mathcal{S}$. The shape $\mathcal{S}$ can always be found by considering two parameters for the part of interest: (1) D_{min}: the smallest gap through which the part will fit and (2) D_{max}: the maximum distance between any two points on the part. Therefore, for any given part, the circular boundary with radius: $r_{cage} = (1/2)D_{max} + \alpha$ where $\alpha > 0$ is a constant scalar, will always contain the object. This is referred to as the *caging* circle. For a given r_{cage} and D_{min}, there must be at least $N_{min} > 0$ number of robots to ensure object closure.

We have shown that this approach will not work reliably at the micro-scale in [30]. While the center of mass of the part does indeed remain inside the caging circle boundary during the duration of the transport tests, positioning errors corresponding to about 20% of the path distance of the transport test exist along with large changes in part orientation values (as much as 90° in some cases). This is because in the original formulation [28] for defining the r_{cage} and N_{min} values, circular robots with a finite radius are used. At the micro-scale, point robots (manipulator probes) are being used instead. Larger size robots (end-effectors) would provide more contact area with and protrude into the cage, essentially limiting the free space in the cage that the part can move during the transport primitive. This will, in turn, reduce the parts' positioning and orientation errors (changes) during the transport task. This information, along with the fact that we are manipulating objects at the micro-scale with small assembly tolerances, requires instead that a tighter cage needs to be used for robust transport of the micro-scale part.

In order to define caging grasps for robust micro-scale transport in a systematic way, we take inspiration from parallel jaw grippers and utilize the part geometries to define a tight caging polygon on the micro-part that we can translate in the workspace. The guiding principle behind parallel jaw grippers is that they apply pinching grasp forces to a part. The gripping force (F_g) from one jaw contact has an opposing equivalent force from the other jaw (Fig. 3(left)). We want our cage to be able to exert forces (F_c) with a similar opposing force equivalents in order to hold the orientation and position of the part inside the cage during transport as much as possible. This can be done by defining an appropriate caging polygon about the part (Fig. 3(right)). To determine where to position the N_i (≤ 4) manipulator tips to form the caging polygon, we examine the geometry of the part of interest. First, we identify the location and number of convex corners (cc) and non-convex corners (ncc) of the part. It is assumed that the probe will apply a caging force in-line with the center of the convex corner. Therefore, we define *corner normals* to each convex and non-convex corner as n_{cc} and n_{ncc}, respectively, to describe the line of action for the caging forces. The corner normals bisect the complimentary angle defined by the convex corner and are

angled towards the inside of the part. We also define a caging force circle with radius γ. Caging force circles are centered at the location where an extended corner normal intersects with an opposing side of the part. With these definitions and information, we can examine the cases when the number of convex corners on the part varies between 0, 1, and > 1. Note: there may be cases when not all of the N probes are needed to form an appropriate caging polygon.

Number of Convex Corners = 1

- Place N_1 at cc_1.
- Insert a caging force circle with radius γ where the n_{cc_1} intersects with the opposite boundary of the part.
- If a ncc is located inside the caging force circle (γ-region), place N_2 and N_3 on the borders of the diameter of the circle where they intersect with the part. This is shown in the top left (row 1, column 1) of Fig. 4.
- If no ncc are in the γ-region, place N_2 and N_3 inside the γ-region along the edge of the part.

Number of Convex Corners > 1

- Examine all cc locations and their corresponding γ-regions on the part.
- If there are zero pairs of cc locations with overlapping γ-regions (i.e.: cc located in a different cc's γ-region), place N_1 at cc_1 and N_2 on the part inside the γ-region corresponding to n_{cc_1} (see Fig. 4 row 2, column 1).
- If there are two cc locations with overlapping γ-regions, place N_1 and N_2 at cc_1 and cc_2 (see Fig. 4 row 3, column 1).
- Connect a line between N_1 and N_2 and draw a perpendicular line to it at the midpoint. Draw two γ-regions where the perpendicular intersects the edges of the part in opposite directions.
- If a cc resides inside these γ-regions, place N_3 and/or N_4 at these locations (see N_3 and N_4 in Fig. 4 row 3, column 1).
- If a cc is not inside a γ-region, place N_3 and/or N_4 along the part somewhere inside these regions (see N_4 in Fig. 4 row 2, column 1).

Number of Convex Corners = 0

- Examine all ncc locations and their γ-regions
- If there is a ncc inside a γ-region, place N_1 and N_2 along the part at the intersection of the γ-region circle and part boundary. Then place N_3 and N_4 along the part at the intersection of the γ-region circle for that particular ncc. (see Fig. 4 row 4, column 1)
- If there are no ncc's inside a γ-region, draw a γ-region around one of the ncc's and place N_1 and N_2 along the part the two places where the circle intersects with the part boundary. Then place N_3 along the part inside the actual γ-region for the chosen ncc. Connect a line from the ncc to N_3 and draw a perpendicular to it at the midpoint. Place N_4 along the part where the perpendicular intersects with the part boundary.

Arranging the manipulator probes in this manner will ensure that opposing caging force equivalents are exerted during the transport primitive. We call cages defined in this way *feature-defined (FD) cages*. Fig. 4 shows FD-cages generated using this methodology for four micro-parts of interest. The double arrows in the figure represent the caging forces (F_c) resulting from the FD-cages. The single

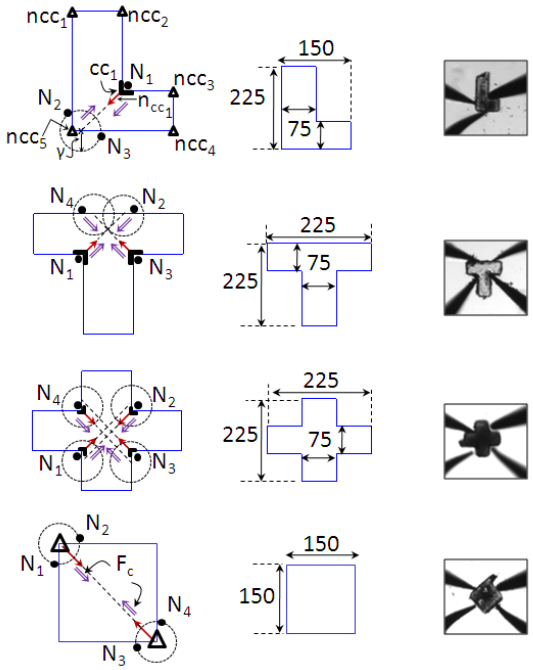

Fig. 4. FD-cages (left), dimensioned parts in microns (middle), and images of FD-cages with microscope (right).

arrows represent the corner normals. Triangles are used to identify ncc's, while the right angled-shapes represent the cc's. The filled-in circles designate the locations for the manipulator probes. The values for γ were chosen as γ= L/4, where L is the characteristic length of the part. Dimensional information for the parts as well as images of the parts in the microrobotics test-bed (Fig.2(a)) are also provided in Fig. 4.

C. Error Bounds

It is not required or desired here to have a force closure grasp in order to transport the part. It's actually advantageous at the micro-scale not to have constant contacts with the part during a transportation manipulation primitive in order to reduce the effects of the dominant surface forces at these length scales. The intermittent contacts that the cage provides during transport helps mitigate these. Thus, the FD-cage will impart all of the constraints necessary for robust transport. However, since we are not enforcing strict point contacts with the part at all times during transport, and also due to the uncertainty in the system when positioning the probes, some errors (or play) in part positioning and orientation during transport will occur (exist). These errors will be bounded based on the ϵ distance away from the part that we place our probes. For the four parts of interest in this study, we will encounter two types of caging polygon shapes - a rectangle and a triangle. These are shown schematically in Fig. 5. There is an ϵ ring surrounding the caging polygons that is the free region inside the cage that the part can move about during transport. Therefore, the $X-$ and $Y-$axis position accuracy for the part is bounded by ΔXY_{max}= 2ϵ. The error bounds for the rotation angle θ_p are a function of the size and shape of caging polygon as well as the ϵ value. For the rectangular and triangular cages, the maximum orientation changes are given by the following equations, respectively: $\Delta\theta_{max}^{Rect} = min\{\sin^{-1}(\epsilon/w), \sin^{-1}(\epsilon/h)\}$ and $\Delta\theta_{max}^{Tri} = min\{\sin^{-1}(2\epsilon/w), \sin^{-1}(3\epsilon/2h)\}$.

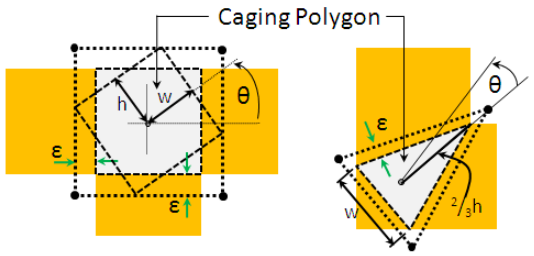

Fig. 5. Error bound analysis diagrams for rectangular (left) and triangular (right) caging polygons

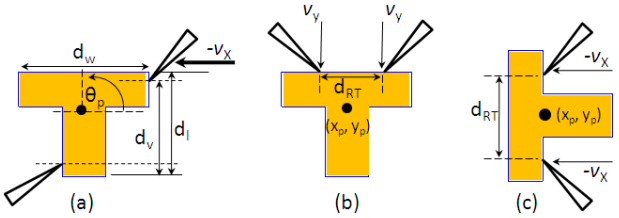

Fig. 6. (a) Rotational and (b) One-sided Pushing (OSP) X-direction and (c) Y-direction translation primitives.

IV. MICROASSEMBLY TASK PLANNING

Our approach to microassembly tasks consist of constructing manipulation plans of three types of primitives to robustly control the position and orientation of the part of interest. The three primitives utilized are: *Caging Transport*, *Rotation*, and *One-Sided Pushing Translation*. The manipulation plans generated initially call for a rotation primitive to orientate the part to the final goal orientation. Next, a caging primitive will be used to transport the part from it's location to an orthogonal location a characteristic length distance away from the goal location. Finally, a short one-sided pushing (OSP) $X-$ or $Y-$axis translation primitive is executed to position the part into it's final goal location in the assembly. The caging transport primitive has been described in Sec. III-A. The rotation and OSP primitives will be summarized now.

1) Rotation: The rotational motion primitive [32] consists of one stationary manipulator probe and one active manipulator probe (Fig. 6(a)). They are positioned symmetrically above and below the center of mass of the part of interest with a vertical separation distance, d_v, according to: $max(d_w, d_l) \geq d_v \geq min(d_w, d_l) \cdot (3/4)$ where d_w and d_l are the length and width dimensions of the part, respectively. Once in position, the active probe is translated along the X-axis causing the part to pivot around the stationary probe's tip at the base of the part.

2) One-Sided Pushing 1D Translation: Following the caging transport primitive, the part is in it's final orientation a short orthogonal distance from the goal position. A one-sided pushing (OSP) 1D translation either in the X or Y direction can be used to translate the part to the goal position [30]. These are used in instances when a caging transport primitive cannot be because the manipulator probes surrounding the part will interfere with part mating or with another part already in the assembly or workspace. OSP translation is performed using two manipulators forming a two-point contact about the center of mass the part along one side to reliably control it's position. The separation distance for the OSP translation primitives, d_{RT}, is given by: $d_{RT} = d_L(1/2)$ where d_L is the length of the side of the part that is being pushed, as shown in Fig. 6(b) and 6(c).

V. EXPERIMENTAL RESULTS

A. Experimental Setup

The microrobotics test-bed used here is shown in Fig. 2(a). It consists of an inverted optical microscope (Nikon Ti-U), automated XY stage with encoders (Nikon Ti-S-ER), CCD camera (QImaging Retigna 200R), and four computer-controlled manipulators (Sutter Instruments MPC-285), and customized controllers. A custom LabView-based control program was development to allow for real-time vision position feedback and simultaneous control of all the manipulators in the system. The manipulators are outfitted with tungsten probes with 5 μm diameter tips. Manipulation and assembly tests were performed on parts made from SU-8 photoresist (*www.microchem*) with the planar dimensions shown in Fig. 4. The part thicknesses are about 100 μm. A 4X objective was used in the microscope along with a 1.5X zoom providing a field of view of approximately 2100 μm X 2800 μm. The camera images provide a resolution of about 7 μm/pixel. Using this test-bed, experimental caging manipulation transport tests for each part were conducted as well as the representative assembly task executed.

B. FD-cage Transport Test Results

At least three caging transport motion primitive tests were performed on the four micro-parts of Fig. 4. The FD-cages for the tests were determined using the methodology presented in Sect. III-B and are shown schematically in the middle column of Fig. 4. For each trial, the cage was used to transport the part in a 500 μm $\times$ 500 μm box pattern in the workspace and the x_p, y_p, and θ_p trajectories for the parts captured with the vision system. Fig. 7 shows these part trajectories overlaid on the nominal translational and rotational trajectories for the transport task. The nominal XY trajectory is a perfect 500 μm $\times$ 500 μm square path, while the nominal change in the θ_p coordinate is zero. In addition to this trajectory data, the average ΔX_{max}, ΔY_{max}, and $\Delta\theta_{max}$ values from the trials for the position and orientation errors of the micro-parts were extracted. This data is reported in Table I. From observing the data in this table along with the trajectories in Fig. 7, we can see that the FD-cage is able to robustly transport all of the micro-parts tested along a desired path (x_p,y_p) with a limited (bounded) change in orientation (θ_p) of the parts. This data is consistent with our error bound analysis presented in Sec. III-C. For these experiments, it reasonable to assume an ϵ ring value of at least 2 pixels, corresponding to a value of 14 μm. We can accurately position the probe tips in the workspace to $\pm$ 1 pixel resolution, corresponding to a value of 14 μm. Therefore, we can examine the error bounds for the FD-cages based on ϵ values of 14 μm and 28 μm, respectively. The first case corresponds to perfect probe positioning while the second corresponds to probe positioning accuracy with a $\pm$ 1 pixel error. Results from this analysis is shown in Table II. By comparing this table with the data in Table I, we can see that the ΔX_{max}, ΔY_{max}, and $\Delta\theta_{max}$ values from the experiments are all within the predicted error bounds. It should be noted that the error bounds are proportional to the size of the caging polygon. Therefore, smaller parts with smaller caging polygons are susceptible to larger errors. This is the case with the *T*-shape and *Cross* parts. Since their caging polygons dimensions (75μm $\times$ 75 μm) are smaller

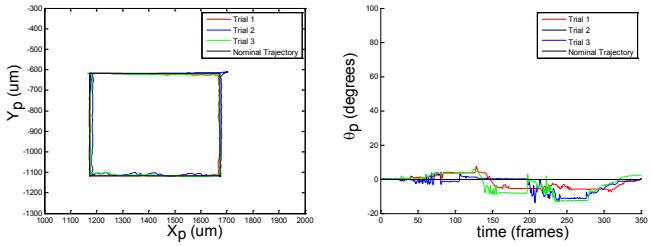

(a) L-shaped Part: x_p,y_p Trajectories (b) L-shaped Part: θ_p Trajectories

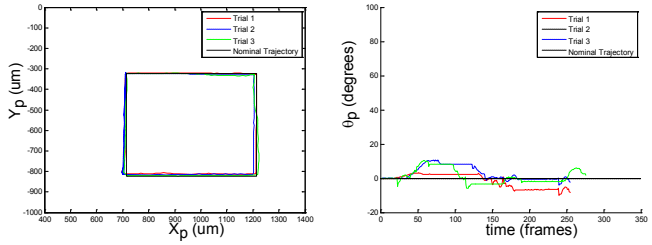

(c) T-shaped Part: x_p, y_p Trajectories (d) T-shaped Part: θ_p Trajectories

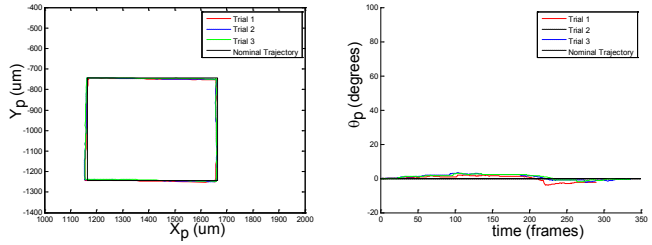

(e) Cross Part: x_p,y_p Trajectories (f) Cross Part: θ_p Trajectories

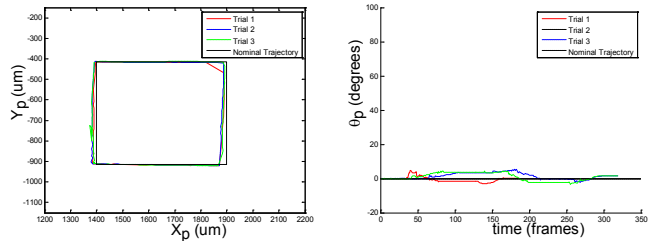

(g) Square Part: x_p, y_p Trajectories (h) Square Part: θ_p Trajectories

Fig. 7. FD-Caging Transport Part Trajectories

TABLE I

FD-CAGE PART TRANSPORT EXPERIMENTAL RESULTS

Part	Ave ΔX_{max} and ΔY_{max} $x_p(\mu m)$	$y_p(\mu m)$	Ave $\Delta\theta_{max}$ (°)
L-shape	9	13	17
T-shape	14	12	15
Cross	11	6	5
Square	28	6	8

than the other parts, the ϵ value is a larger percentage of the caging polygon which results in larger bounded error values. In the case of the FD-cage transport tests on the *Square* shaped parts, there exists a preferred orientation of θ_p=45° for optimal results. This configuration is shown in the bottom right of Fig. 4. This is due to the fixed angles (θ_1 to θ_4) of the probes in the manipulation system. In this fixed configuration, the probes are not able to form the required resultant opposing force equivalents needed to robustly control the part during transport when θ_p=0°. This limitation of the test-bed should be incorporated into the FD-caging grasp planning algorithm and noted when planning sequences of motion primitives for microassembly tasks.

TABLE II

ERROR BOUNDS FOR FD-CAGING PART TRANSPORT

Part	ϵ (μm)	w (μm)	h (μm)	ΔXY_{max} (μm)	$\Delta\theta_{max}$ (°)
L-shape	14	57	140	28	9
L-shape	28	57	140	56	17
T- & Cross	14	38	38	28	22
T- & Cross	28	38	38	56	48
Square	14	27	80	28	10
Square	28	27	80	56	21

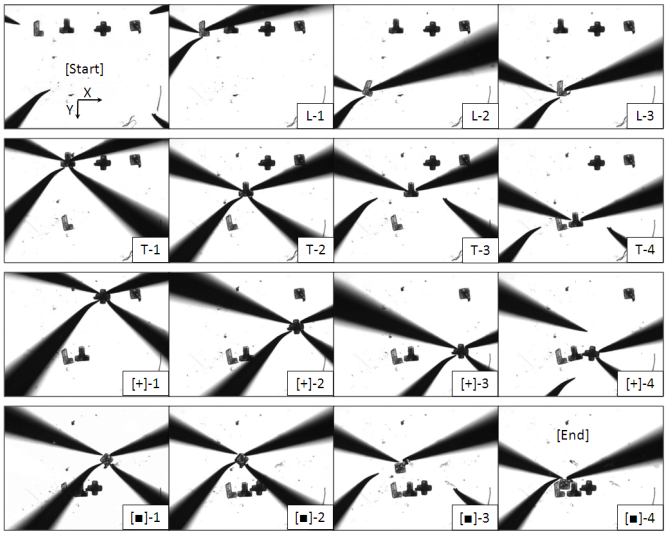

Fig. 8. Microassembly experiment snap-shots

C. Microassembly Test Results

Experiments were performed utilizing the FD-cage transport, rotational, and OSP translational primitives for the microassembly task shown in Fig. 1. Snap-shots from the experiments are shown in Fig. 8. It was assumed that the parts have already been rotated to their goal orientation so only caging transport and OSP primitives are needed to execute the task. However, due to the limitations of the fixed manipulator probe angles, the *Square* part was transported at angle of $\theta_p = 45°$ and then a rotational primitive applied before the final OSP operation to move it to it's goal location. The assembly plan calls for positioning the parts in the following order: *L*-shape, *T*-shape, *Cross*, and *Square*, with the following sequence of moves. Note: references to snap-shots in Fig. 8 are provided for each sequence.

L-part Transport: 1000 μm in Y (L-1 to L-2)
Transport: 500μm in X (L-2 to L-3)

T-part Transport: 500 μm in Y (T-1 to T-2)
Transport: 250 μm in X (T-2 to T-3)
OSP: 1000 μm in Y (T-3 to T-4)

Cross Transport: [Diagonal] 500 μm in X, 500 μm in Y ([+]-1 to [+]-2)
Transport: 415 μm in Y ([+]-2 to [+]-3)
OSP: -310 μm in X ([+]-3 to [+]-4)

Square Transport: -450 μm in X ([■]-1-[■]-2)
Rotation: 135° ([■]-2-[■]-3)
OSP: 350 μm in Y ([■]-3-[■]-4)

All of the prescribed caging transport primitives worked as expected. Problems were encountered when executing the OSP primitives in the case of the *Cross* and *Square* parts. The presence of a left-over tab on these parts from the manufacturing process also caused difficulties when trying to manipulate the parts into their goal locations. The OSP

operation on the *Cross* induced a slight rotation of the part. This coupled with the tab on the mating side of the piece in the assembly caused part interference during the tests as shown in snap-shot [+]-4. The presence of the tab on the *Square* part required a large rotational primitive ($135°$) for the part that was hard to achieve robustly. The tab also was disruptive for the OSP move, again causing part rotation that inhibited successful final assembly. To prevent this problem, an additional probe was positioned in a strategic location to prevent this rotation and help guide the part into the final configuration, as seen in snap-shot [■]-4. Additionally, the low aspect ratio ($\sim$ 1:1) of the parts made the execution of the OSP and rotational primitives difficult as they were more 3D than actually planar parts. Furthermore, errors can be attributed to scratches and dirt on the supporting substrate, probe tip mis-alignment in the workspace and tip curvature changes as some tips were slightly bent during the course of testing. None-the-less, the transport primitives with the FD-cages worked as expected and show great promise for robustly transporting micro-scale objects throughout the workspace. The error bounds can be used along with task tolerances in order to successfully plan microassembly tasks.

VI. CONCLUSIONS

In this paper, we have developed a systematic method to determine feature-defined caging grasps on micro-scale, planar, polygonal parts. These grasps are used to create caging polygons around the micro-part in order to execute a micromanipulation caging transport primitive. We have shown theoretical error bounds for the transport primitive with the feature-defined cages based on this methodology. This information is critical when planning microassembly tasks. Experimental results show that FD-cages determined in this manner are able to robustly transport four different types of micro-parts and exhibit errors in the predicted bounds. Finally, this primitive has been used in conjunction with a rotational and one-sided-pushing primitive to successfully perform a representative microassembly task.

REFERENCES

[1] J. Cecil, D. Vasquez, and D. Powell, "A review of gripping and manipulation techniques for micro-assembly applications," International Journal of Production Research, vol. 43, no. 4, pp. 819–828, February 2005.

[2] J. Feddema, P. Xavier, and R. Brown, "Micro-assembly planning with van der Waals force," Proceedings of the IEEE International Symposium on Assembly and Task Planning (ISATP '99), pp. 32 –38, July 1999.

[3] Y. Zhou and B. Nelson, "The effect of material properties and gripping force on micrograsping," in Proceedings of the IEEE International Conference on Robotics & Automation (ICRA), San Francisco, CA, April 2000.

[4] C. Keller, "Microgrippers with integrated actuator and force sensors," in Proceedings of the World Automation Congress, 1998, pp. 217–222.

[5] J. Cecil and N. Gobinath, "Development of a virtual and physical cell to assemble micro devices," Special Issue of the Journal of Robotics and CIM, pp. 431–441, August-October 2005.

[6] J. Alex, B. Vikramaditya, and B. Nelson, "A virtual reality teleoperator interface for assembly of hybrid MEMS prototypes," Proceedings of DETC98 1998 ASME Engineering Technical Conference, Atlanta, GA, Sept. 13-16 1998.

[7] T. Kasaya, H. Miyazaki, S. Saito, and T. Sato, "Micro object handling under SEM by vision-based automatic control," Proceedings of the IEEE International conference on Robotics and Automation, Detroit, MI, pp. 2189–2196, 1999.

[8] A. Das, P. Zhang, W. Lee, D. Popa, and H. Stephanou, "μ^3: Multiscale, deterministic micro-nano assembly system for construction of on-wafer microrobots," in IEEE International Conference on Robotics and Automation (ICRA), Rome, Italy, April 2007.

[9] R. Fearing, "Survey of sticking effects for micro parts handling," IEEE/RSJ Int. Conf. on Intelligent Robotics and Sys.(IROS), Pittsburgh, PA, vol. 2, pp. 212–217, August 5-9 1995.

[10] K. Boehringer, R.Fearing, and K. Goldberg, Handbook of Industrial Robotics, 2nd Ed. John Wiley and Sons, 1999, ch. Microassembly, pp. 1045–1066.

[11] M. Moll, K. Goldberg, M. Erdmann, and R. Fearing, "Orienting micro-scale parts with squeeze and roll primitives," IEEE Int. Conf. on Robotics and Automation, Washington, DC, May 11-15 2002.

[12] M. Mason, "Manipulator grasping and pushing operations," Ph.D. dissertation, Massachusetts Institute of Technology, 1982.

[13] ——, "Mechanics and planning of manipulator pushing operations," International Journal of Robotics Research, vol. 5, no. 3, pp. 53–71, 1986.

[14] M. Peshkin and A. Sanderson, "The motion of a pushed, sliding object, Part 1: Sliding friction," Robotics Institute, Carnegie Mellon University, Pittsburgh, PA, Tech. Rep. CMU-RI-TR-85-18, September 1985.

[15] K. Lynch and M. Mason, "Dynamic nonprehensile manipulation: Controllability, planning, and experiments," International Journal of Robotics Research, vol. 18, no. 1, pp. 64–92, January 1999.

[16] P. Song, J. Pang, and V. Kumar, "A semi-implicit time-stepping model for frictional compliant contact problems," International Journal for Numerical Methods in Engineering, Accepted for publication 2004.

[17] J. Trinkle, S. Berard, and J. Pang, "A time-stepping scheme for quasistatic multibody systems," International Symposium of Assembly and Task Planning, July 2005.

[18] M. Salganicoff, G. Metta, A. Oddera, and G. Sandini, "A vision-based learning method for pushing manipulation," AAAI Fall Symp. on Machine Learning in Computer Vision., 1993b.

[19] Z. Balorda, "Reducing uncertainty of objects by robot pushing," IEEE Int. Conf. on Robotics and Automation, pp. 1051–1056, 1990.

[20] K. Lynch and M. Mason, "Stable pushing: Mechanics, controllability, and planning," International Journal of Robotics Research, vol. 15, no. 6, pp. 553–556, December 1996.

[21] M. Savia and H. Koivo, "Contact micromanipulation-survey of strategies," Mechatronics, IEEE/ASME Transactions on, vol. 14, no. 4, pp. 504–514, Aug. 2009.

[22] B. Vikramaditya and B. Nelson, "Visually guided microassembly using optical microscopes and active vision techniques," IEEE Int. Conf. on Robotics and Automation, Albuquerque, New Mexico, 1997.

[23] K. Kosuge, Y. Hirata, H. Kaetsu, and K. Kawabata, "Motion control of multiple autonomous mobile robots handling a large object in coordination," IEEE Int. Conf. on Robotics and Automation, pp. 2666–2673, May 1999.

[24] D. Rus, "Coordinated manipulation of objects in a plane," Algorithmica, vol. 19, no. 1, pp. 129–147, 1997.

[25] T. Sugar and V. Kumar, "Multiple cooperating mobile manipulators," IEEE Int. Conf. on Robotics and Automation, pp. 1538–1543, 1999.

[26] M. Mataric, M. Nilsson, and K. Simsarian, "Cooperative multi-robot box-pushing," IEEE/RSJ Int. Conf. on Intelligent Robots and Systems, pp. 556–561, 1995.

[27] G. Pereira, V. Kumar, and M. Campos, "Decentralized algorithms for multi-robot manipulation via caging," The Int. Journal of Robotics Research, vol. 23, no. 7/8, pp. 783–795, 2004.

[28] J. Fink, M. A. Hsieh, and V. Kumar, "Multi-robot manipulation via caging in environments with obstacles," in 2008 IEEE International Conference on Robotics and Automation, Pasedena, CA, May 2008.

[29] J. Fink, N. Michael, and V. Kumar, "Composition of vector fields for multi-robot manipulation via caging," Robotics: Science and Systems III, 2007.

[30] D. Cappelleri, M. Fatovic, and U. Shah, "Caging micromanipulation for automated microassembly," Proceedings of the IEEE International Conference on Robotics and Automation, to appear, Shanghai, China, May 2011.

[31] D. Cappelleri, J. Fink, B. Mukundakrishnan, V. Kumar, and J. Trinkle, "Designing open-loop plans for planar micro-manipulation," IEEE Int. Conf. on Robotics and Automation, Orlando, FL, May 2006.

[32] P. Cheng, D. Cappelleri, B. Gavrea, and V. Kumar, "Planning and control of meso-scale manipulation tasks with uncertainties," in Proceedings of Robotics: Science and Systems, Atlanta, GA, USA, June 2007.

[33] D. Cappelleri, C. Peng, J. Fink, B. Gavrea, and V. Kumar, "Automated assembly for meso-scale parts," IEEE Transactions on Automation Science and Engineering, *to appear*, 2011.

[34] V. K. Peng Cheng, Jonathan Fink, "Abstractions and algorithms for cooperative multiple robot planar manipulation," in Proceedings of Robotics: Science and Systems IV, Zurich, Switzerland, June 2008.

[35] M. Spong, S. Hutchinson, and M. Vidyasagar, Robot Modeling and Control. John Wiley & Sons, Inc., 2006.